

Additive Effects on Chemical Vapor Deposition of CdS

Yung-Jung Hsu and Shih-Yuan Lu*

*Department of Chemical Engineering, National Tsing-Hua University, Hsin-Chu, TAIWAN 30043,
Republic of China*

Abstract

An additive, silver nitrate (AgNO_3), was used to prepare nanostructured films of cadmium sulfide (CdS) via a metallorganic chemical vapor deposition (MOCVD) process by using a single source precursor of CdS. The silver (Ag) vapors or clusters resulting from the thermal decomposition of the additive served as the extra active sites for nucleation of both surface and gas-phase growth of CdS and had an apparent influence on the morphology and photoluminescent (PL) property of the resulting CdS deposits. When the additive was present, a reduction in characteristic size of the CdS deposit structure was observed. In the first half of the reactor, an apparent morphology change and a significant increase in the deposition rate of CdS deposits were observed, attributable to the increased nucleation rate. In the second half of the reactor, both deposit morphology and deposition rate did not change much, possibly due to the depletion of Ag vapors or clusters. The PL quantum yield of the deposit was much enhanced in the additive case. In addition, the gas-phase formed particles became more numerous and much finer in size due to the increased nucleation rate. The nanoparticles collected at the reactor exit were smaller than 5 nm, giving rise to a substantial blue-shift in ultraviolet/visible (UV/Vis) absorption (from 500 to 375 nm) and corresponding photoluminescence (from 520 to 430 nm) spectra because of the strong quantum confinement effect.

Keywords: additive effect, chemical vapor deposition, CdS, single-source precursor

1. Introduction

Thin films of II-VI semi-conductors such as cadmium sulfide (CdS) and zinc sulfide (ZnS) are technologically important for their potential applications in optical coating, solid-state solar cell windows, optoelectronic devices, and light-emitting diodes (Berrigan et al., 1998; Tsuji et al., 2000; Uda et al., 2003). Deposition processes for semiconductor films can be roughly divided into two categories: those carried out through gas phase routes (Berrigan et al., 1998; Tsuji et al., 2000; Uda et

* Corresponding author: Tel: +886-3-571-4364 ; Fax: +886-3-571-5408

E-mail address: sylu@mx.nthu.edu.tw

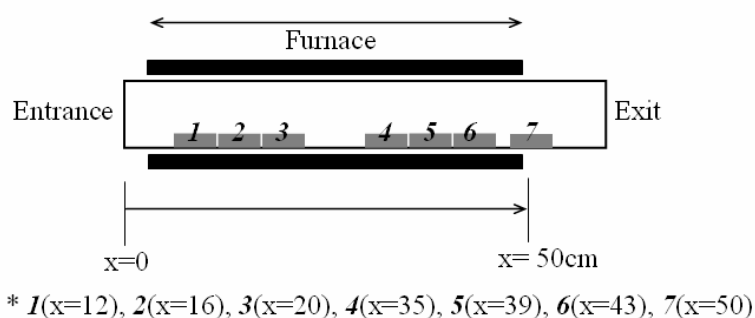


Figure 1.a Schematic of the tubular CVD reactor with the seven collection positions identified. The entrance of the tubular reactor was set as the origin.

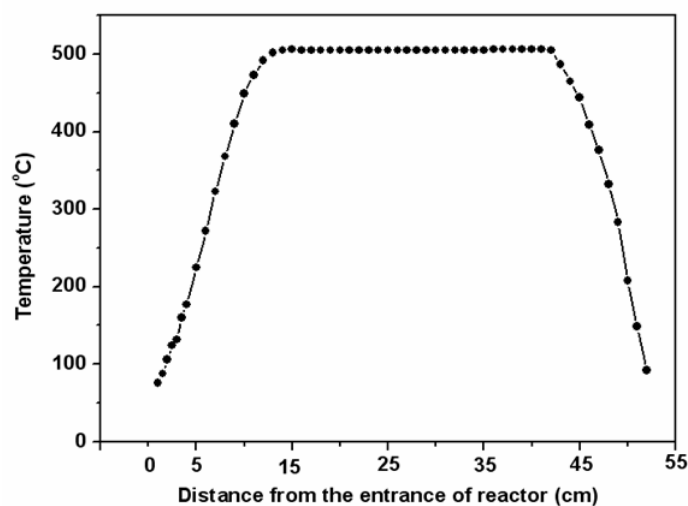


Figure 1.b Temperature distribution of the three-zone furnace with the temperature set at 500 °C.

al., 2003) and those through liquid phase routes (Boyle et al., 1999; Boone and Shannon, 1996). Gas phase routes, such as metalorganic chemical vapor deposition (MOCVD), offer the advantage of easier end-product separation, higher throughput rate, and purer product, and have thus become more popular.

Thin films of nanostructured CdS were prepared with a hot-wall MOCVD process by using a single-source precursor of CdS. In addition, an additive, silver nitrate (AgNO_3), was introduced the system to study its effect on the morphology and optical properties of the resulting CdS deposits. It has been demonstrated that, through introduction of an additive in the CVD growth process, a reduction in reaction temperature (Zheng et al., 1998) and the selective suppression of gas-phase reaction (Takahashi et al., 1995) can be achieved. This study focuses on the effect of an additive on the morphology and optical properties of a deposit.

Conventionally, CVD processes for preparing II-VI compound semiconductors employ separate metal and chalcogen sources, which are independently introduced into the reactor. In recent years, single-source precursors, which are chemical compounds containing both metal and chalcogen

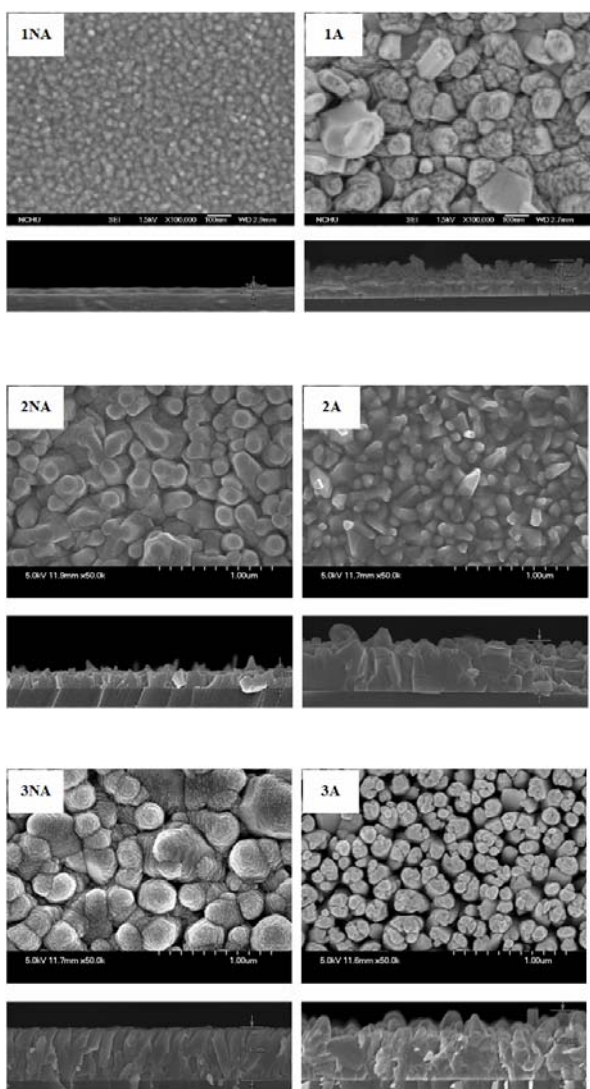


Figure 2. Top and side view SEM graphs of CdS deposits collected from locations 1, 2, and 3 for both Case NA and Case A.

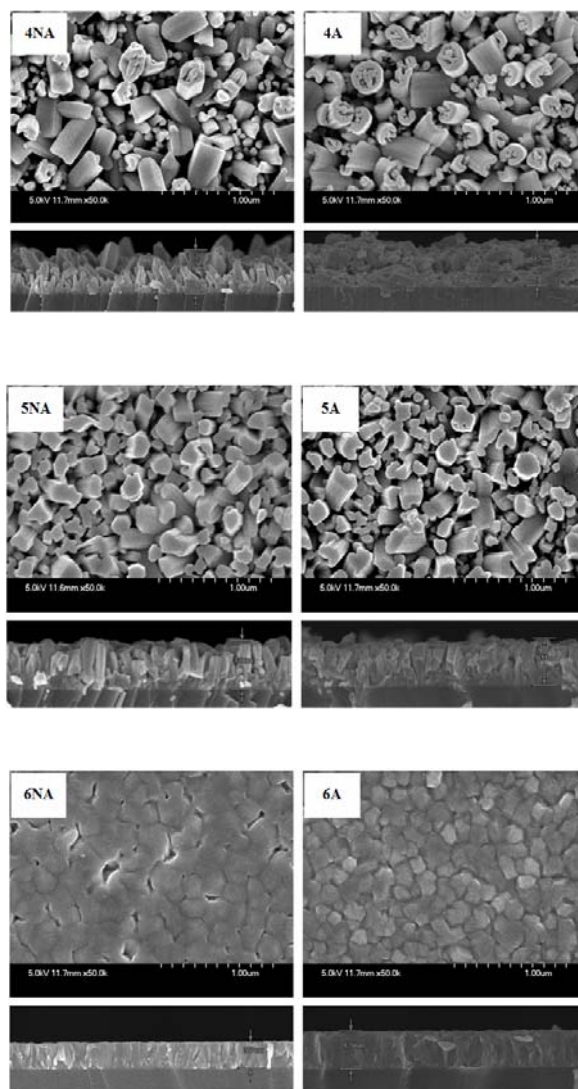


Figure 3. Top and side view SEM graphs of CdS deposits collected from locations 4, 5, and 6 for both Case NA and Case A.

sources and give desired compound semiconductors upon thermal decomposition, were developed as a more effective and easier to handle precursor for CVD processes (Motevalli et al., 1996). In this study, a single-source precursor, cadmium dipropyldithiocarbamate ($\text{Cd}(\text{S}_2\text{CNProp}_2)_2$), was used to prepare nanostructured CdS particle films.

2. Experimental Section

Synthesis of single-source precursor. To prepare the single-source precursor of CdS, cadmium hydroxide ($\text{Cd}(\text{OH})_2$), N-dipropyl amine (HNProp_2), and carbon disulfide (CS_2) of stoichiometric proportion were mixed to react in boiling ethanol for 2 hr. The product was purified using the recrystallization process, and the desired single-source precursor, $\text{Cd}(\text{S}_2\text{CNProp}_2)_2$, was obtained.

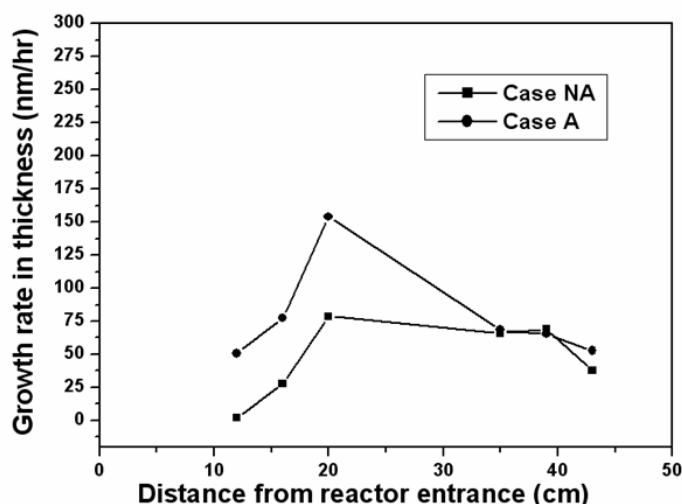


Figure 4. Comparison in growth rate distribution along the axial direction of the reactor for Case A and Case NA.

MOCVD process for preparation of nanostructured films of CdS. MOCVD was conducted in a simple, reduced-pressure (30 torr), hot-wall reactor. Amorphous quartz plates were used as the substrate for the deposition of CdS films. Seven samples of CdS deposits were collected from seven different locations along the tubular reactor (Figure 1[a]) to study the possible variation of morphology, optical property, and additive effect in the axial direction of the main reaction stream. The first three collecting substrates were placed in the first half near the entrance of the reactor, the next three in the second half near the exit of the reactor, and the last one at the reactor exit. The reactor was heated with a three-zone furnace offering a 30-cm isothermal zone. The temperature distribution along the tubular reactor (set at 500 °C) is depicted in Figure 1(b).

The precursor and the additive, AgNO₃, were placed in two different pre-heating zones that were heated to appropriate temperatures (160 °C for the precursor and 200 °C for AgNO₃) to generate vapors. The weight loss rates for the precursor and additive in the deposition were 0.04 g/hr and 0.003 g/hr, respectively, and the corresponding mole concentrations, calculated based on the ideal gas law, were 1.12×10^{-7} gmole/L and 2.30×10^{-8} gmole/L, respectively. The vapors of the precursor and additive were introduced into the furnace by the carrier gas N₂. The furnace temperature was set at 480 °C. All depositions were run at a carrier gas flow rate of 200 sccm and a system pressure of 30 torr for 10 hr.

Characterization. UV/Vis absorption spectra were obtained using a Hitachi U-3300 spectrophotometer. For photoluminescence (PL) spectroscopy, a Hitachi F-4500 equipped with a xenon lamp (150W) and a 700V photomultiplier tube as detector was used. Both absorption and photoluminescence spectra were obtained at room temperature under ambient atmosphere. The solvent used to suspend the nanoparticles deposited on location 7 was acetone.

Photoluminescence quantum yields (Q_s) of the samples were determined from the following expression (Hitachi Scientific Instrument Technical Data):

$$Q_s = Q_{st} (A_{st}/A_s) (D_s/D_{st})$$

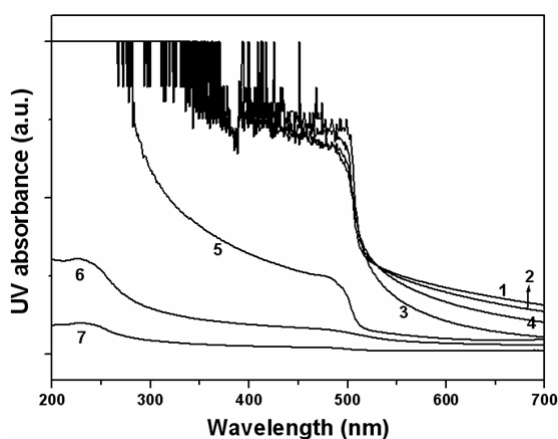


Figure 5.a

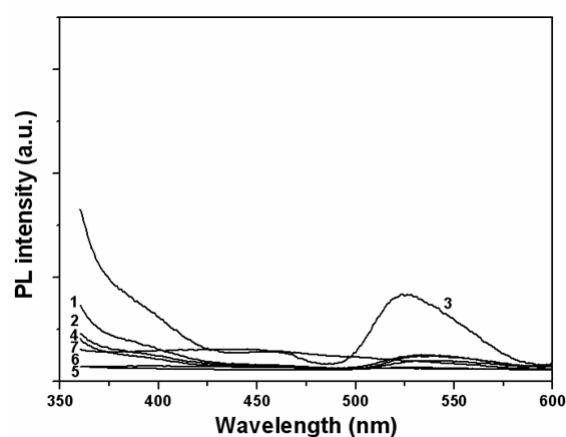


Figure 6.a

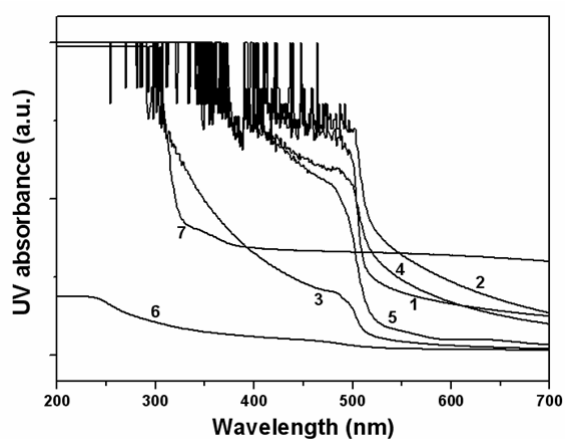


Figure 5.b

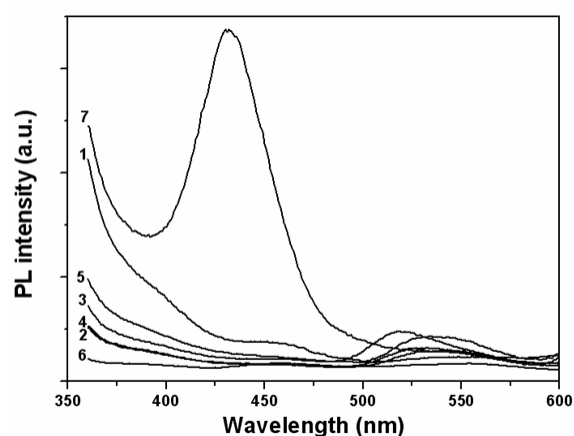


Figure 6.b

Figure 5. UV-Vis absorption spectra of CdS deposits (a) without and (b) with the additive.

Figure 6. PL emission spectra of CdS deposits (a) without and (b) with the additive.

Here, Q_{st} is the quantum yield of the reference standard substance, tryptophan, known to be 0.16 at a concentration of $0.73 \mu\text{g/mL}$ in H_2O ; A_{st} and A_s are the absorbance values of the tryptophan solution and sample, respectively, at the wavelength of 320 nm; and D_s and D_{st} are the corresponding integrated wavenumber values for the sample and tryptophan, respectively, in the PL spectra.

Scanning electron microscopy (SEM) graphs were taken with a Hitachi S-4700 operated at an accelerated voltage of 5 kV. All samples were sputtered with thin layers of gold (Au) before analysis. Transmission electron microscopy (TEM) graph was taken with a JEOL JSM-1200EX operated at 80 kV.

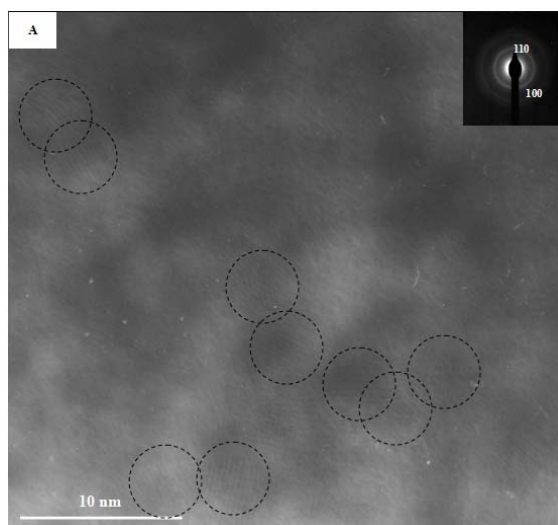


Figure 7.a HRTEM images of collected CdS nanoparticles at location 7 for Case A.

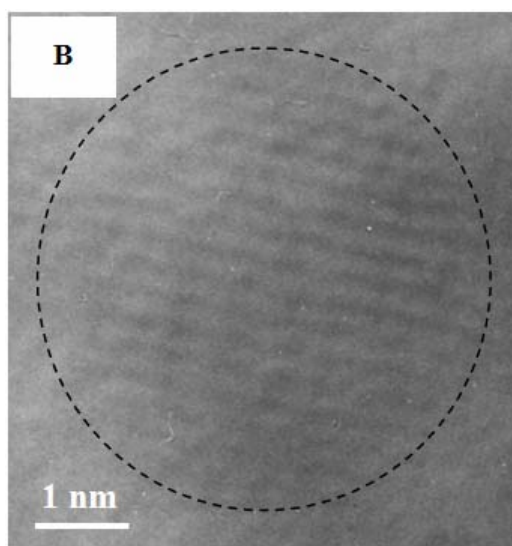


Figure 7.b The insert was the corresponding select area electron diffraction (SAED) pattern for the nanoparticles.

3. Results and Discussion

The case of “no additive” is referred to as Case NA and the case of “with additive” is referred to as Case A. All deposits collected within the reactor (locations 1 to 6) adhered to the substrates firmly and with the appearance of a film, while those collected at the reactor exit (location 7) were loose agglomerates of CdS nanoparticles. This observation, together with later SEM graphs, implied that surface reaction and growth dominated at locations within the reactor (locations 1-6), while the substrates at location 7 collected particles formed in the gas phase and deposited onto the collecting substrates. In Figures 2 and 3, top and side view SEM graphs of the deposits collected from locations 1-6 reveal the variation in morphology due to collecting position and additive addition. Among the 12 samples, sample 1NA (location 1, Case NA) appears to be particle film, while all other samples can

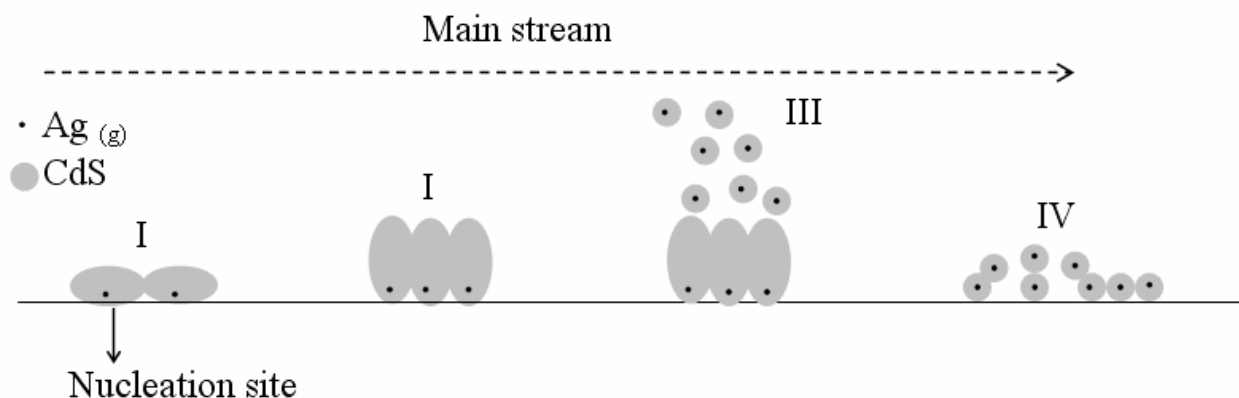


Figure 8. Schematic for growth mechanism in growing CdS deposits by using AgNO_3 as the additive.

be described more appropriately as rod-woods. The difference in appearance with respect to the additive was dramatic for the first three samples collected from the first half of the reactor, while the morphology of samples from locations 4-6 remained the same, except that the average characteristic size shrunk in the presence of the additive. For samples from locations 2 and 3, the average characteristic size of the structure shrunk in addition to the morphology change. Sample 1A seems to possess a structure of much larger characteristic size. But if examined closely, the rods of sample 1A possessed a much finer grain structure, with the characteristic size about the same as that of sample 1NA.

The extent of morphology change correlated with the deposition rate. Figure 4 presents the deposition rate in terms of thickness growth rate as determined from the side view SEM graphs and deposition time. Evidently, the deposition rate at the first three locations increased dramatically, while that at locations 4-6 remained almost unchanged.

In addition to morphology and deposition rate, the possible effects of the additive on the optical properties of the deposits was studied. Figure 5 shows the absorption spectra for CdS deposits collected from the seven locations of both cases. For both absorption and PL measurements, film samples were used directly for deposits from locations 1 to 6, while colloidal suspensions were prepared for deposits from location 7. All samples, except 7A, showed an absorption edge at around 500 nm, which is the absorption edge for CdS (corresponding to an energy band gap of 2.5 eV) without quantum confinement effect (Figure 5). When the characteristic size of the deposit is less than or comparable to the exciton Bohr radius of the material ($\sim 3\text{nm}$ for CdS), quantum confinement effect arises leading to a widening of the energy band gap and a corresponding blue shift in the absorption edge. That was observed for sample 7A. A substantial blue shift, from 500 to 375 nm, implied the smallness of the characteristic size of the deposit. For an absorption edge of 375 nm, one can estimate the characteristic size of the deposit by using Brus' equation (Brus and Rossetti, 1984), and the result is 3 nm, equal to the exciton Bohr radius of CdS. Note here the absorption edges of samples 6NA, 7NA, and 6A were not clearly revealed due to the scale limit.

Table 1. Enhancement in quantum yield of photoluminescence at different locations of the reactor achieved through addition of the additive.

	Case NA	Case A	Enhancement
	Q_s	Q_s	$[(Q_s)_A - (Q_s)_{NA}] / (Q_s)_{NA} \times 100\%$
1	0.0054	0.0114	111
2	0.0027	0.0043	59.3
3	0.0199	0.0283	42.2
4	0.0046	0.0051	10.9
5	0.0014	0.0060	329
6	0.0036	0.0560	1460
7	0.0032	0.0607	1800

For the corresponding PL spectra, all samples but sample 7A showed the typical near band edge emission of bulk CdS at around 520 nm (Figure 6). Sample 7A, however, showed a strong PL emission peak at around 430 nm, near the absorption edge of 375 nm (Figure 5[b]). Figure 7 shows the HRTEM image of the CdS nanoparticles of sample 7A, revealing a particle size of less than 5 nm. The direct observation of the particle size from the TEM graph agreed well with that from the estimation of Brus' equation. The insert of Figure 7 shows the electron diffraction pattern of CdS particles, and also shows that the particle was in its hexagonal crystalline phase. Also, a high quantum yield of 6.07% was achieved for sample 7A, while that for corresponding sample 7NA was only 0.32%. In fact, the amount of deposit for sample 7NA was almost non-detectable, while that for sample 7A was abundant. The deposition rate at location 7 was also dramatically increased. Table 1 lists the PL quantum yields of the CdS deposits collected from the seven locations for both cases and the corresponding enhancement ratios of Case A over corresponding Case NA. The enhancement ratio dropped first from location 1, reached a minimum at location 4, and increased from there on. At location 4, the additive effect was the least among all seven locations in terms of variation in morphology, deposition rate, and, consequently, PL efficiency. The enhancement ratio in PL quantum yield seems to correlate with the extent of morphology change, appearance and characteristic size, achieved with the additive. It is worth mentioning that some nanoparticles also deposited on location 6A, boosting the PL enhancement even further.

The role played by the additive is explained in Figure 8. AgNO_3 , once introduced into the deposition chamber, thermally decomposed to result in Ag vapors or clusters. These Ag vapors or

clusters, some depositing onto the substrate and some remaining in the gas phase, served as active sites for nucleation of CdS deposits. The nucleation rate of CdS was thus increased, leading to the formation of more and finer particles or rods and an increase in the deposition rate. The enhancement effect in deposition rate was more pronounced for the leading part of the reactor, and was much less for the downstream portion of the reactor, since the Ag vapors or clusters were generated and consumed mainly in the upstream. This also explains why the morphology change at locations 1-3 was more dramatic. In addition, because of the Ag vapors or clusters, the gas-phase formed particles increased in number and became finer in size, so that a dramatic increase in deposition rate and substantial blue shift in the absorption edge was observed. The physics behind the enhancement in PL efficiency due to an additive remains unclear at this stage and needs further study.

4. Conclusion

The effect of an additive in enhancing the deposition rate and PL efficiency of a CdS deposit was demonstrated. It was also demonstrated that morphology change can be induced through the use of an additive. The main role played by the additive was to supply extra nucleation active sites to promote nucleation and subsequent growth of the targeted material. It is expected that this kind of additive effect would apply to other material systems, including ceramics and other semiconductors.

Acknowledgement

The authors gratefully acknowledge the support of the National Science Council of the Republic of China under NSC grant 91-2214-E-007-014.

References

- Berrigan R. A., Maung N., Irvine S. J. C., Cole-Hamilton D. J., and Ellis D. (1998), Thin films of CdTe/CdS grown by MOCVD for photovoltaics, *J. Cryst. Growth* 195: 718-724.
- Boone B. E., and Shannon C. (1996), Optical Properties of Ultrathin Electrodeposited CdS Films Probed by Resonance Raman Spectroscopy and Photoluminescence, *J. Phys. Chem.* 100: 9480-9484.
- Boyle D. S., O'Brien P., Otway D. J., and Robbe O. (1999), Novel approach to the deposition of CdS by chemical bath deposition: the deposition of crystalline thin films of CdS from acidic baths, *J. Mater. Chem.* 9: 725-729.
- Brus L. E., and Rossetti R. (1984), Size effects in the excited electronic states of small colloidal CdS crystallites, *J. of Chem. Phys.* 80: 4464-4469.
- Hitachi Scientific Instrument Technical Data, FL No.24.
- Motevalli M., O'Brien P., Walsh J. R., and Watson I. M. (1996), Synthesis, Characterization and X-ray Crystal Structures of Asymmetric Bis(dialkyldithiocarbamates) of Zinc: Potential Precursors

for ZnS Deposition, *Polyhedron* 15: 2801-2808.

Takahashi T., Egashira Y., and Komiyama H. (1995), Control of SiH₄/O₂ chemical vapor deposition using the gas-phase additive C₂H₄, *Appl. Phys. Lett.* 66: 2858-2860.

Tsuji M., Aramoto T., Ohyama H., Hibino T., and Omura, K. (2000), Characterization of CdS thin film in high efficient CdS/CdTe solar cells, *J. Cryst. Growth* 214: 1142-1147.

Uda H., Yonezawa H., Ohtsubo Y., Kosaka M., and Sonomura H. (2003), Thin CdS films prepared by metalorganic chemical vapor deposition, *Sol. Energy Mater. Sol. Cells* 75: 219-226.

Zheng L. X., Yang H., Xu D. P., Wang X. J., Li X. F., Li J. B., Wang Y. T., Duan L. H., and Hu X. W. (1998), Low-temperature growth of cubic GaN by metalorganic chemical-vapor deposition, *Thin Solid Films* 326: 251-255.

Received for review, September 01, 2003

Accepted, October 31, 2003